Future Integrative Medicine **2025** vol. 000(000) | 000–000 Epub
DOI: 10.14218/FIM.2025.00031

Original Article

Ganoderma lucidum Alleviates High-fat Diet-induced Hepatic Lipotoxicity via Modulating the Unfolded Protein Response and Endoplasmic Reticulum-phagy

Chenxi Cao, Suwei Jin, Hongbin Song, Yingying Guo, Fangrui Cao, Yongguang Liu, Tianji Xia, Shanshan Zhang, Qi Chang* and Mingzhu Yan*

Institute of Medicinal Plant Development, Chinese Academy of Medical Sciences and Peking Union Medical College, Beijing, China

Received: May 29, 2025 | **Revised:** July 18, 2025 | **Accepted:** August 12, 2025 | **Published online:** September 30, 2025

Abstract

Background and objectives: A long-term high-fat diet (HFD) exerts lipotoxic effects on multiple organs, particularly the liver, leading to metabolic diseases. This study aimed to delineate the dynamic effects of HFD on lipid metabolism, elucidate the mechanisms underlying hepatic lipotoxicity, and investigate the protective effects of *Ganoderma lucidum* against lipotoxicity both *in vitro* and *in vivo*.

Methods: C57BL/6 mice were fed either a 45% or 60% HFD, followed by measurements of body composition, serum lipid profile, and liver pathology at four, eight, twelve, and sixteen weeks. Inflammatory responses, the unfolded protein response (UPR), and endoplasmic reticulum (ER)-phagy were examined in the livers of mice at 16 weeks. Male C57BL/6 mice were randomly assigned to four groups (n = 12 per group): normal diet, 45% HFD, and two HFD + *Ganoderma lucidum* water extract (GLE) groups (1 g/kg/d and 2 g/kg/d of crude drug, orally administered by gavage for eight weeks following a four-week HFD induction).

Results: Body weight, body fat, serum lipids, and hepatic steatosis increased progressively, accompanied by impaired glucose tolerance and liver injury, as indicated by elevated serum alanine aminotransferase (ALT) and aspartate aminotransferase (AST) levels. HFD also induced activation of the STING and NF-κB signaling pathways, as well as the PERK and IRE1 branches of the UPR. Similarly, ER-phagy selective receptors, particularly FAM134B, which is primarily expressed in hepatocytes as shown by single-cell sequencing, were upregulated after 16 weeks of HFD feeding. Furthermore, GLE mitigated palmitic acid-induced lipotoxicity in primary hepatocytes, as evidenced by improved cell viability, reduced ALT, AST, and lactate dehydrogenase levels in the culture supernatant, and decreased transferase dUTP nick-end labeling-positive cell counts. In 45% HFD-fed mice, GLE reduced serum total cholesterol, low-density lipoprotein, and hepatic triglyceride levels.

Conclusions: HFD-induced lipotoxicity causes hepatic tissue injury and inflammatory responses, which may be alleviated by coordinated regulation of compensatory UPR and ER-phagy. *Ganoderma lucidum* shows promise as a dietary supplement for managing metabolic disorders.

Keywords: High-fat diet; Lipotoxicity; Unfolded protein response; Endoplasmic reticulum-phagy; ER; *Ganoderma lucidum*.

***Correspondence to:** Mingzhu Yan and Qi Chang, Institute of Medicinal Plant Development, Chinese Academy of Medical Sciences and Peking Union Medical College, 151 Malianwa North Road, Haidian District, Beijing 100193, China. ORCID: https://orcid.org/0000-0002-5806-1602 (MY); https://orcid.org/0000-0001-9546-1827 (QC). Tel: +86-10-57833468 (MY); +86-10-57833224 (QC), E-mail: mzyan@implad.ac.cn (MY); qchang@implad.ac.cn (QC)

How to cite this article: Cao C, Jin S, Song H, Guo Y, Cao F, Liu Y, *et al*. *Ganoderma lucidum* Alleviates High-fat Diet-induced Hepatic Lipotoxicity via Modulating the Unfolded Protein Response and Endoplasmic Reticulum-phagy. *Future Integr Med* 2025;000(000):000–000. doi: 10.14218/FIM.2025.00031.

Introduction

Saturated fatty acids, such as palmitic acid (PA), are abundant in animal fats, dairy products, and vegetable oils.[1] A long-term high-fat diet (HFD) rich in saturated fatty acids induces lipotoxicity, which exerts detrimental effects on multiple organs and systems, leading to a constellation of metabolic diseases, including hyperlipidemia, type 2 diabetes mellitus, metabolic dysfunction-associated steatotic liver disease (MASLD), and atherosclerosis.[2,3] These metabolic diseases are now among the

most prevalent worldwide and represent major threats to public health.[4] Multiple studies have shown close epidemiological associations between them, as well as intertwined mechanisms, among which lipotoxicity is a unifying and defining factor that drives HFD-induced metabolic dysfunction.[5] For example, the hallmark of MASLD is the excessive accumulation of fat (primarily triglycerides) and free fatty acids in the liver, leading to hepatocellular lipotoxicity manifested as oxidative stress, endoplasmic reticulum (ER) stress, activation of inflammatory pathways, and impairment of autophagy. These intracellular events are mutually regulated, forming a vicious cycle that induces cell death and promotes the progression of MASLD.[3,6] Therefore, understanding the molecular details of lipotoxicity provides critical insights for developing intervention strategies against HFD-associated metabolic diseases, especially as new signaling pathways continue to emerge. ER-phagy, a form of selective autophagy targeting damaged ER, represents a novel adaptive mechanism in response to ER stress, in addition to the canonical unfolded protein response (UPR).[7] An *in vitro* study has demonstrated that ER-phagy is induced in HepG2 cells following oleic acid treatment to prevent lipoapoptosis,[8] but whether it is activated *in vivo* and its associated regulatory molecules remain unknown.

Ganoderma lucidum (*G. lucidum*), as defined in the Pharmacopoeia of the People's Republic of China (2020 edition), refers to the dried sporocarp of *Ganoderma lucidum* (Curtis) P. Karst. or *Ganoderma sinensis* Zhao, Xu et Zhang. Chemical analyses have revealed that *G. lucidum* contains approximately 400 bioactive components, including polysaccharides, triterpenoids, nucleosides, steroids, fatty acids, and various trace elements, which contribute to its therapeutic effects on various diseases.[9] As a renowned medicinal fungus, *G. lucidum* has a long history of dietary use and is recognized for its beneficial effects on longevity,[10] immunomodulation,[11,12] and metabolic disorders.[13–15] Previous studies have shown that *G. lucidum* alleviates HFD-induced hepatic steatosis in mice.[16,17] However, a clinical trial reported that *G. lucidum* failed to improve hyperglycemia, hypertension, or hyperlipidemia in patients with metabolic syndrome or diabetes.[18] These conflicting findings prompted us to further investigate the potential effects of *G. lucidum* in HFD-fed mice, focusing on its ability to ameliorate lipotoxicity, a key driver of hepatocyte death.

This study aimed to investigate the dynamic effects of 45% and 60% HFDs on lipid metabolism in mice, with particular emphasis on the activation of the UPR and its downstream ER-phagy pathways in metabolic dysregulation. Furthermore, we evaluated the therapeutic potential of *G. lucidum* against lipotoxicity in both primary hepatocytes and HFD-induced murine models, thereby providing mechanistic insights and potential intervention strategies for metabolic liver disease.

Materials and methods

Preparation of G. lucidum water extract (GLE)

G. lucidum was collected from the Ta-pieh Mountains, Anhui Province, China. Dried *G. lucidum* (200 g) was cut into small pieces and wrapped in a gauze bag, followed by decoction with 4 L of distilled water for 1 h. This process was repeated three times. The pooled extracts were filtered and concentrated to a final volume of 200 mL by vacuum evaporation to obtain GLE (equivalent to 1 g crude drug/mL). The final GLE solution was stored at −80 °C for future use. A small portion of GLE was evaporated to dryness and weighed, yielding an extraction efficiency of 7.17% (w/w).

Chromatographic analysis of GLE

An aliquot of 0.1 mL of GLE was heated, dried, re-dissolved in 1 mL of methanol, and filtered to prepare the sample. The chemical components in GLE were analyzed using a high-performance liquid chromatography-ultraviolet system (Waters e2695, Milford, MA, USA). Chromatographic separation was performed on a Thermo Accucore XL C18 column (150 × 4.6 mm, 4 μm) maintained at 25°C. The injection volume was 5 μL. The mobile phase consisted of 0.1% acetic acid in water (A) and acetonitrile (B), with the following linear gradient program: 0–20 m, 20–35% B; 20–30 m, 35% B; 30–35 m, 35–65% B; 35–40 m, 65% B; 40–45 m, 65–20% B. The flow rate was 0.8 mL/m, and the detection wavelength was set at 254 nm. Authentic standards of ganoderic acids A, B, C1, C2, and ganodermanontriol (purity ≥ 98%) were purchased from ChemFaces (Wuhan, China).

Animal experiments

All animal procedures were approved by the Animal Ethics Committee of the Institute of Medicinal Plant Development, Chinese Academy of Medical Sciences, and Peking Union Medical College (SLXD-20210930022), and conducted in accordance with the guidelines of the committee. The study protocols complied with the Animal Research: Reporting of *In Vivo* Experiments (ARRIVE) guidelines. Male C57BL/6 mice (20–22 g) were purchased from Beijing Vital River Laboratory Animal Technology Co., Ltd. The mice were acclimatized in new cages (n = 4 per cage) for seven days with free access to water. They were maintained at an ambient temperature of 23–25 °C, humidity of 50%–60%, and a 12:12 h light/dark cycle (lights on at 8:00 am, off at 8:00 pm).

To establish the hepatic lipotoxicity model, 36 mice were randomly assigned to three groups (n = 12 per group): normal chow diet (ND), 45% HFD, and 60% HFD. The ND group received a standard chow diet (Xietong Bio-Engineering Co. Ltd., SWS9102, Jiangsu, China), while the other two groups were fed 45% or 60% HFD (Trophic Animal Feed High-Tech Co. Ltd., TP23100, TP23300, Jiangsu, China) for 16 weeks. The diet formulations are shown in Table 1. At the end of the experiment, mice were weighed and anesthetized for blood and liver tissue collection.

For the GLE treatment experiments, 48 mice were randomly divided into four groups: ND, 45% HFD, and two GLE-treated groups (1 and 2 g crude drug/kg, respectively, based on the Chinese Pharmacopoeia). For gavage, concentrated GLE was diluted to 0.1 and 0.2 g/mL with distilled water. After four weeks of HFD feeding, GLE was administered orally once daily at 0.2 mL/20 g for eight weeks. ND and 45% HFD mice received equivalent volumes of water by gavage.

Measurement of body weight, feed intake, and body composition

Mice were weighed weekly. Feed was weighed twice weekly and replaced with fresh feed each time. Body composition was measured using a Bruker Minispec Body Composition Analyzer (Billerica, MA, USA).

Oral glucose tolerance test

A 4–6 h daytime fast has been reported to sufficiently lower blood glucose, reduce gastric contents, and ensure clearance of food consumed during the dark phase.[19] After 16 weeks of feeding, mice were orally administered glucose (2 g/kg) following a 6 h fast. Blood glucose was measured from the tail vein at 0, 15, 30, 60, and 120 m post-gavage using an Accu-Chek Performa blood glucose meter. The area under the curve (AUC) was calculated using the following equation:

Table 1. Diet formulations

Class description	45% HFD		60% HFD	
	Ingredients	Weight (g/kg)	Ingredients	Weight (g/kg)
Protein	Casein	175	Casein	267
	L-Cystine	2	L-Cystine	4
Carbohydrate	Corn Starch	132	/	/
	Maltodextrin	125	Maltodextrin	157
	Sucrose	202	sucrose	89
Fat	Soybean oil	30	Soybean oil	33
	Lard	196	lard	301
Fiber	Cellulose	62	Cellulose	67
Mineral	Mineral Mix, M1021	61	Mineral mix, M1020	66
Vitamin	Vitamin Mix, V1010	12	Vitamin mix, V1010	13
	Choline bitartrate	3	Choline bitartrate	3
Food additives	TBHQ	0.045	TBHQ	0.067
	Total	1,000	Total	1,000

HFD, high-fat diet; TBHQ, *tert*-butyl hydroquinone.

$$\text{AUC (mmol/L*m)} = \frac{(G0+G15)\times 15}{2} + \frac{(G15+G30)\times 15}{2} + \frac{(G30+G60)\times 30}{2} + \frac{(G60+G120)\times 60}{2}$$

where G represents the blood glucose level at the indicated time point.

Serum and liver biochemical analyses

Serum levels of total triglycerides (TG), total cholesterol (TC), alanine aminotransferase (ALT), aspartate aminotransferase (AST), high-density lipoprotein cholesterol (HDL-C), and low-density lipoprotein cholesterol (LDL-C) were measured using a fully automated biochemistry analyzer (Beckman Coulter AU480, Brea, CA, USA) with commercially available assay kits (BioSino, 100020090, 100020080, 100020003, 100020013, 100020238, 100020248, Beijing, China). A portion of liver tissue was homogenized using a fully automated tissue grinder (Shanghai Jingxin, JXFSTPRP-L, Shanghai, China). The homogenate was centrifuged at 1,000 × g for 10 m, and the supernatant was analyzed for TG and TC levels using commercial assay kits (Nanjing Jiancheng, A110-1-1, A111-1-1, Nanjing, China).

Histological analyses

Liver tissues were dissected and fixed in 4% paraformaldehyde for 24 h. After dehydration, tissues were embedded in paraffin and sectioned at 5 μm thickness. Sections were stained with hematoxylin and eosin (H&E). For Oil Red O staining, frozen liver sections were processed as previously described.[20] The MASLD activity score was determined based on the histological scoring system proposed by the Pathology Committee of the MASH Clinical Research Network.[21]

Western blotting

The protocol for western blotting was described in our previous study.[22] Briefly, ~20 mg of frozen liver tissue was lysed and homogenized in 400 μL radio immunoprecipitation assay lysis buffer containing 1% protease and phosphatase inhibitor cocktail (100×). Following centrifugation, the protein concentration of the supernatant was determined using a bicinchoninic acid protein assay kit (Solarbio, PC0020, Beijing, China) and adjusted to 2.5 μg/μL. Ten microliters of denatured protein was separated on 10% or 12% sodium dodecyl sulfate-polyacrylamide gel electrophoresis and electrophoretically transferred to nitrocellulose membranes. Membranes were blocked with 5% nonfat milk in tris buffered saline with Tween-20 (TBST) for 1 h at room temperature and then incubated with primary antibodies at 4°C with shaking overnight. The antibodies used in this study are listed in Table S1. After washing three times with TBST (5 m each), membranes were incubated with secondary antibody (1:5,000) for 1 h at room temperature. Protein bands were visualized using an enhanced chemiluminescent reagent kit (Beyotime Biotech, P0018FS, Shanghai, China) with a ChemiDoc™ Imager (Bio-Rad, Hercules, CA, USA). Band intensities were quantified using ImageJ software (Java 8, NIH) and normalized to total protein or β-actin. All western blot analyses were performed in triplicate for each antibody to ensure reproducibility. In some cases, membranes were stripped using stripping buffer (SW3020, Solarbio) to allow detection of additional targets.

Quantitative reverse transcription-polymerase chain reaction

Total RNA was extracted from liver tissues using TRIzon reagent (CWBIO, CW0580S, Jiangsu, China). A total of 1.5 μg RNA was reverse-transcribed into cDNA using the *TransScript*® All-in-One First-Strand cDNA Synthesis Kit (TransGen, AT341, Beijing, China) according to the manufacturer's instructions. Target gene expression was quantified using a CFX96 Touch Real-Time PCR Detection System (Bio-Rad, Hercules, CA, USA) with *TransStart*® Top Green qPCR SuperMix (TransGen, AQ131, Beijing, China) and normalized to *β-actin* mRNA levels. Primers were purchased from Sangon Biotech (Shanghai, China) and are listed in Table 2.

Primary hepatocyte isolation, culture, and treatment

The isolation procedure for primary mouse hepatocytes was adapt-

Table 2. Primer sequences for quantitative reverse transcription-polymerase chain reaction

Genes	Forward primer (5′–3′)	Reverse primer (5′–3′)
Ccl2	TTTTTGTCACCAAGCTCAAGAG	TTCTGATCTCATTTGGTTCCGA
Cxcl10	ATGACGGGCCAGTGAGAATG	ATGATCTCAACACGTGGGCA
Il-6	TCCATCCAGTTGCCTTCTTG	TTCCACGATTTCCCAGAGAAC
Tnf	ATGTCTCAGCCTCTTCTCATTC	GCTTGTCACTCGAATTTTGAGA
β-actin	GTGCTATGTTGCTCTAGACTTCG	ATGCCACAGGATTCCATACC

Ccl2, C-C motif chemokine ligand 2; *Cxcl10*, C-X-C motif cchemokine ligand 10; *Il-6*, interleukin-6; *Tnf*, tumor necrosis factor.

ed from our previous study with modifications.[22] Male C57BL/6 mice (six to eight weeks old) were anesthetized with 80 mg/kg pentobarbital sodium. The superior vena cava was ligated, followed by liver perfusion through the inferior vena cava with Hank's balanced salt solution (HBSS) containing 0.5 mM ethylene glycol tetraacetic acid (EGTA). The hepatic portal vein was cut to allow blood outflow. Perfusion was then switched to Dulbecco's Modified Eagle Medium (DMEM)-low glucose (with calcium) containing 100 U/mL collagenase type IV, 1% penicillin/streptomycin, and 15 mmol/L 4-(2-hydroxyethyl)piperazine-1-ethanesulfonic acid (HEPES). The digested liver was excised, minced in DMEM-low glucose with 10% fetal bovine serum (FBS) to terminate collagenase activity, and filtered through a 70 μm strainer. The cell suspension was centrifuged at 50 × g for 10 m. The pellet was resuspended in 90% Percoll solution and centrifuged again at 50 × g to isolate primary hepatocytes.

Cells were seeded and cultured in DMEM-low glucose with 10% FBS for 4 h. After attachment, the medium was replaced with serum-free William's E medium containing 0.1 μmol/L dexamethasone, 15 mmol/L HEPES, 1.25 mg/mL bovine serum albumin (BSA), and 1% insulin-transferrin-selenium (ITS) supplement. Twelve hours after plating, hepatocytes were treated with 0.5 mmol/L PA with or without GLE (10, 20, or 40 mg/mL) for 12 h. Cell viability was assessed using a Cell Counting Kit-8 (Biosharp, BS350B, Anhui, China).

Terminal deoxynucleotidyl transferase dUTP nick-end labeling (TUNEL) assay

A CF488 TUNEL Cell Apoptosis Detection Kit (Servicebio, G1504, Wuhan, China) was used to detect apoptosis in primary hepatocytes treated with or without GLE. Fixed cells were co-stained with Hoechst 33342 (Coolaber, SL7131, Beijing, China) to visualize nuclei. Seven to eight images per group were captured using a Microscope Axio Imager. M2 (ZEISS, Oberkochen, Germany), and the percentage of apoptotic cells was calculated.

Statistical analysis

Data are presented as mean ± standard error of the mean (SEM). The Shapiro–Wilk test was performed in GraphPad Prism (v8.0.2, GraphPad Software, Inc., San Diego, CA, USA) to assess data normality. Statistical significance was determined by one-way or two-way analysis of variance. When analysis of variance indicated significance, post hoc comparisons were performed using Dunnett's test.

Results

Effects of different HFDs on body weight and body composition

C57BL/6 mice were subjected to different HFDs or an ND for 16 weeks to assess the impact of HFDs. From the beginning of feeding to the fourth week, feed intake gradually increased, then slowly declined and stabilized (Fig. 1a). Correspondingly, all mice experienced a rapid growth phase prior to week six, when they were about three months old, after which they entered the mature adult stage (Fig. 1b and c). Although the increase in body weight of ND-fed mice slowed after the sixth week, mice fed HFDs continued to gain weight (Fig. 1b and c). After three weeks of HFD feeding, body weight in the HFD groups was significantly higher than in the ND group. A statistically significant difference in body weight between the 45% and 60% HFD groups appeared only after the eighth week. All mice showed a rapid increase in lean mass by the end of the sixth week of feeding, after which the growth rate slowed (Fig. 1d). HFD feeding did not alter lean mass compared with ND-fed mice. During the feeding period, the fat mass of ND-fed mice increased slightly, from 3.30 ± 0.14 g to 4.59 ± 0.24 g (Fig. 1e), while the fat percentage remained essentially unchanged (Fig. 1f). After 16 weeks of feeding, fat mass in the 45% and 60% HFD groups tripled to 11.36 ± 0.82 g and quadrupled to 18.37 ± 2.62 g, respectively. In contrast to the ND group, the fat percentage in the HFD groups progressively increased, from 15.69 ± 0.50% to 30.60 ± 1.26% in the 45% HFD group, and from 15.53 ± 0.16% to 42.86 ± 4.03% in the 60% HFD group. By the end of the second week, both fat mass and fat percentage in the HFD groups were significantly higher than in the ND group (Fig. 1e and f), with significant differences also observed between the 45% and 60% HFD groups at the same time. Free fluid in ND-fed mice barely changed, whereas it increased over time in the HFD groups, particularly in mice fed the 60% HFD (Fig. 1g).

Effects of different HFDs on glucose and lipid metabolism

After 8 h of fasting, blood glucose levels in mice fed 45% and 60% HFDs were 11.77 ± 0.32 mmol/L and 12.67 ± 0.57 mmol/L, respectively, both significantly higher than those in the ND group (7.30 ± 0.36 mmol/L) (Fig. 2a). After oral administration of 2 g/kg glucose, blood glucose levels in all mice rose rapidly and then gradually declined. At each time point, glucose levels in the HFD-fed groups were significantly higher than in the ND group, and the areas under the curve were correspondingly larger in the HFD groups (Fig. 2b). Moreover, blood glucose levels at 30, 60, and 120 m were higher in the 60% HFD group compared to the 45% HFD group. After four weeks of feeding, serum TC, LDL-C, and HDL-C levels were markedly elevated in the HFD groups compared with the ND group (Fig. 2c–e). By week 8, serum TC and LDL-C levels in the 60% HFD group became significantly higher than in the 45% HFD group (Fig. 2c and d), although levels had been rising since the start of HFD feeding. Conversely, serum TG levels gradually decreased, and by week 16, they were significantly lower in the HFD groups compared with the ND group (Fig. 2f). At

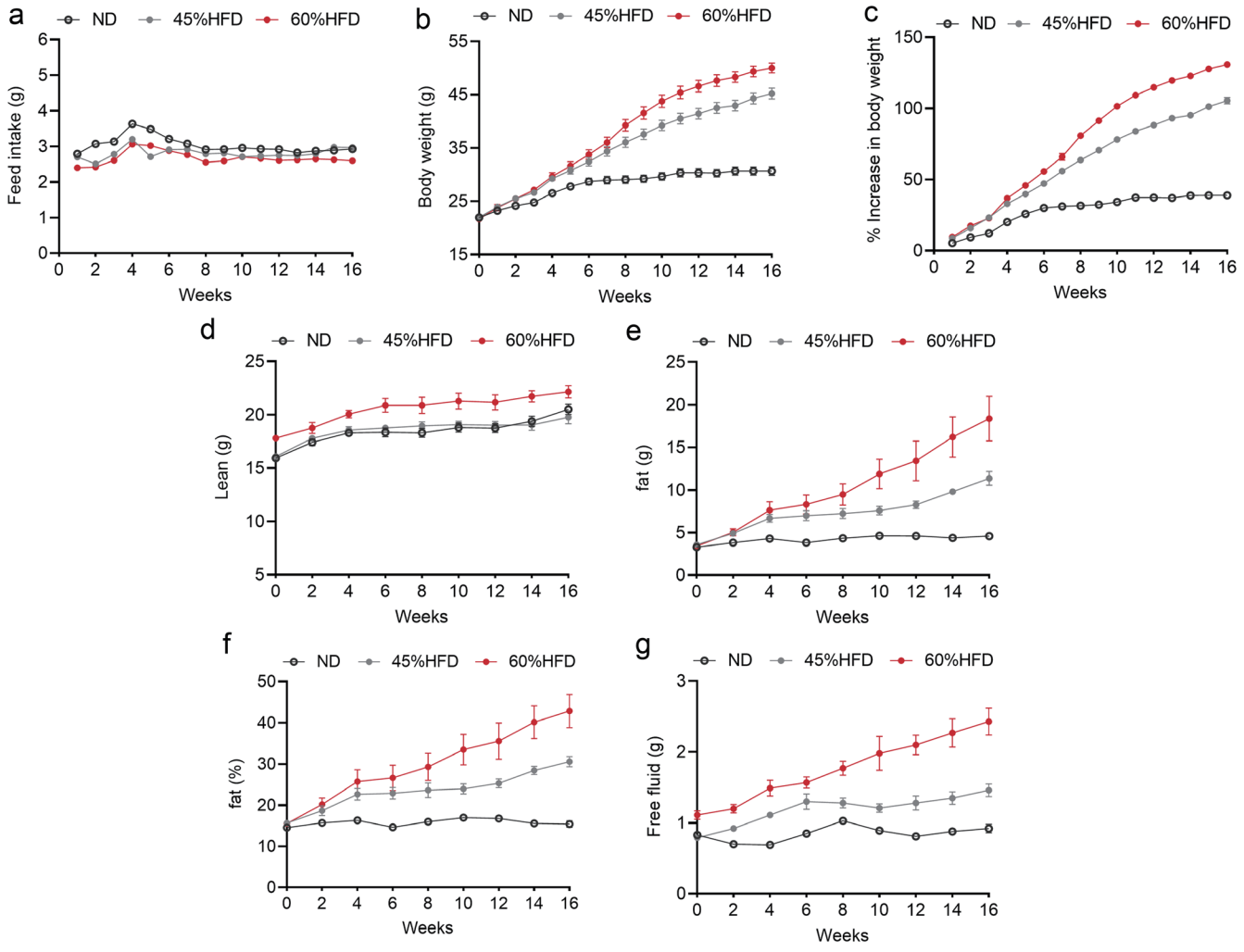

Fig. 1. Changes in weight and body composition after different HFDs. Male C57BL/6 mice were fed an ND, 45% HFD, or 60% HFD for 16 weeks (n = 12). (a) Feed intake, (b) body weight, and (c) percent increase in body weight during the feeding period. The Body Composition Analyzer measured (d) lean mass, (e) body fat, (f) fat percentage, and (g) free fluid at the indicated times (n = 6). Data are shown as mean ± SEM. HFD, high-fat diet; ND, normal chow diet; SEM, standard error of the mean.

weeks 12 and 16, the 60% HFD group displayed higher ALT and AST levels, respectively, compared with the ND group, and these levels were also higher than those in the 45% HFD group, indicating more severe hepatocyte injury (Fig. 2g and h). Collectively, these findings suggest that HFD feeding induces abnormalities in glucose homeostasis and lipid profiles and causes liver injury.

Effects of different HFDs on lipid accumulation in the liver

In terms of gross appearance, the livers of mice fed an ND were dark red in color, with sharp edges and an elastic texture. After 16 weeks of HFD consumption, the red color faded from the enlarged livers and was replaced by pale yellow in the 45% HFD group and yellow in the 60% HFD group (Fig. 3a). In the 60% HFD group, the liver was friable and its edges became blunt (Fig. 3a, right panel). Moreover, both liver size and weight significantly increased, especially in the 60% HFD group (Fig. 3a and b). In contrast, although the liver-to-body weight ratio tended to be higher in the 60% HFD group, it appeared to be significantly lower in the 45% HFD group compared to ND mice (Fig. 3c). Hepatic TG levels increased progressively with 60% HFD feeding (Fig. 3d). Furthermore, 60% HFD induced a dramatic elevation in hepatic TG as early as week 4, whereas a statistically significant increase in the 45% HFD group was not observed until week 16. By week 8, liver TG content in the 60% HFD group was already significantly higher than in the 45% HFD group (Fig. 3d). In the livers of mice fed a 45% HFD, mild to moderate microvesicular steatosis was observed at four, eight, and twelve weeks, as illustrated by H&E (Fig. 3e) and Oil Red O staining (Fig. 3g). Macrovesicular steatosis did not appear until week 16 (Fig. 3e–h). In contrast, in mice fed a 60% HFD, macrovesicular steatosis developed as early as week 12, with larger lipid droplets and broader distribution compared to the corresponding 45% HFD-fed mice (Fig. 3e–h).

Effects of different HFDs on inflammatory response in the liver

Because metabolic stress can trigger inflammation in the liver, we analyzed H&E-stained liver sections to identify pathological signatures of inflammation. Mice fed ND showed normal liver architecture and hepatocyte integrity, with no signs of inflamma-

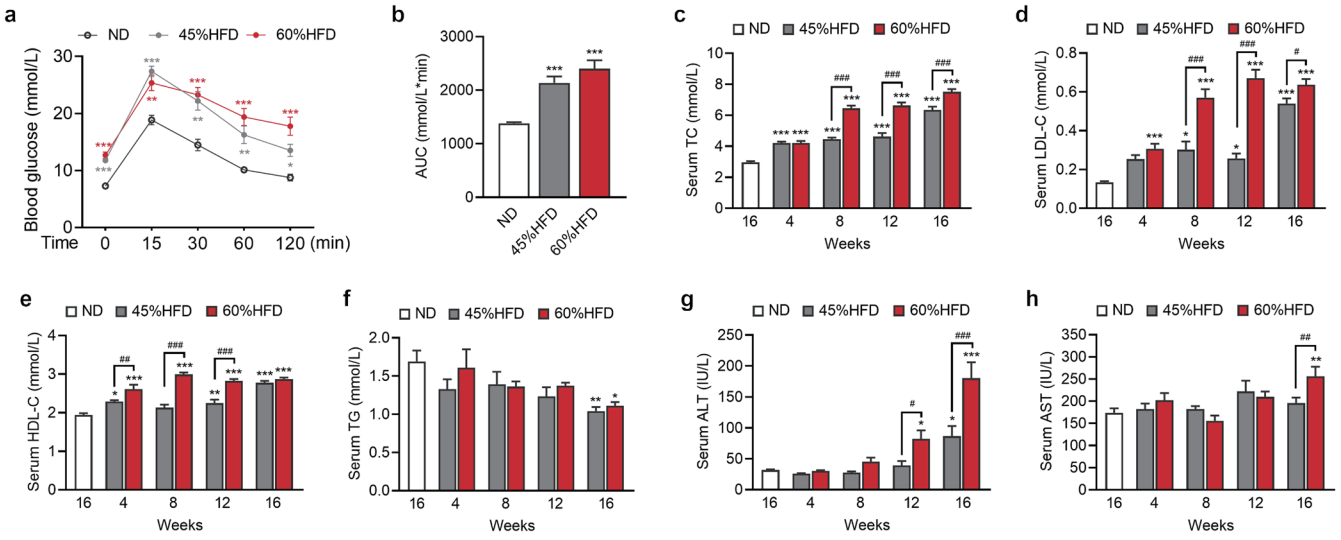

Fig. 2. Effects of different HFDs on serum biochemical indices. After 16 weeks of feeding, (a) oral glucose tolerance tests were performed and (b) the corresponding AUCs were calculated (n = 6). Serum levels of TC (c), LDL-C (d), HDL-C (e), TG (f), ALT (g), and AST (h) in the indicated groups of mice (n = 6–12). Data are shown as mean ± SEM. $^{*}p < 0.05$, $^{**}p < 0.01$, $^{***}p < 0.001$, $^{\#}p < 0.05$, $^{\#\#}p < 0.01$, $^{\#\#\#}p < 0.001$. ALT, alanine aminotransferase; AST, aspartate aminotransferase; AUC, area under the curve; HDL-C, high-density lipoprotein cholesterol; HFD, high-fat diet; LDL-C, low-density lipoprotein cholesterol; SEM, standard error of the mean; TC, total cholesterol; TG, triglycerides.

tion (Fig. 4a, left panel). Apart from steatosis, there were almost no signs of lobular inflammation in mice fed a 45% HFD for 16 weeks (Fig. 4a, central panel). In contrast, inflammatory cell infiltration was evident in the 60% HFD group (Fig. 4a and b). The MASLD activity score (MAS) was calculated based on the extent of steatosis, lobular inflammation, and hepatocyte ballooning. The results showed that only mice fed a 60% HFD for 16 weeks had a strong correlation with a diagnosis of metabolic-associated steatohepatitis (score > 4, Fig. 4c). Differences in MAS scores between the 45% and 60% HFD groups became apparent only after 16 weeks of feeding (Fig. 4c). To further confirm these pathological observations, mRNA levels of *Ccl2*, *Cxcl10*, *Il-6,* and *Tnf* were measured by quantitative reverse transcription-polymerase chain reaction. The data showed that the expression of these hepatic proinflammatory mediators was elevated after 16 weeks of HFD feeding, particularly in the 60% HFD group (Fig. 4d). Although protein levels of stimulator of interferon genes (STING) were significantly increased in both 45% and 60% HFD groups, activation of the IκB kinase beta–nuclear factor-kappa B (IKKβ–NF-κB) signaling pathway signaling cascade was observed only in the livers of mice fed a 60% HFD for 16 weeks (Fig. 4e). Together, these results suggest that feeding mice a 60% HFD for 16 weeks provokes inflammatory responses in the liver.

Effects of different HFDs on ER homeostasis in hepatic cells

Growing evidence suggests that ER stress in the liver is induced by lipotoxicity following HFD feeding.[23] We observed activation of two branches of the UPR in response to HFD-induced ER stress: protein kinase R-like endoplasmic reticulum kinase (PERK) and inositol-requiring enzyme 1 (IRE1) (Fig. 5a–d). Western blot analysis showed that HFD feeding increased the levels of phosphorylated PERK, although statistical significance was only observed between the 60% HFD group and the control group (Fig. 5a and b). In parallel, phosphorylated eukaryotic translation initiation factor 2 alpha (p-eIF2α), downstream of phosphorylated PERK, dramatically increased after 16 weeks of HFD feeding compared to mice fed an ND (Fig. 5a and c). Similarly, the IRE1/c-Jun N-terminal kinase (JNK) signaling pathway was activated in the 60% HFD group, as indicated by increased levels of phosphorylated IRE1 and phosphorylated JNK. In addition to the UPR, ER-phagy is also involved in restoring ER homeostasis under ER stress conditions.[7,24] Single-cell sequencing of mouse liver (https://tabula-muris.ds.czbiohub.org) shows that among ER-phagy receptors, family with sequence similarity 134 member B (*Fam134b*), reticulon 3 (*Rtn3*), and testis-expressed protein 264 (*Tex264*) are mainly expressed in hepatocytes, whereas cell cycle progression 1 (*Ccpg1*) and SEC62 homolog, preprotein translocation factor (*Sec62*) are mainly expressed in hepatic sinusoidal endothelial cells (Fig. 5g). HFD feeding increased the protein levels of ER-phagy receptors, including FAM134B2, CCPG1, SEC62, TEX264, and RTN3 (Fig. 5h). Among these, FAM134B2 in the 60% HFD group showed the greatest increase, with a 2.63-fold elevation compared to the control group (Fig. 5g). Overall, these data suggest that, in addition to the UPR, ER-phagy may play a role in ER quality control in response to HFD-induced lipotoxicity.

GLE protects against lipotoxicity in vitro and in vivo

High-performance liquid chromatography analysis showed the presence of ganoderic acids A, B, C1, and C2, as well as ganodermanontriol, in GLE (Fig. 6a). Among these components, the peak corresponding to ganoderic acid A was the highest, indicating a relatively higher content in GLE, consistent with previous reports.[25] GLE was tested in primary hepatocytes (Fig. 6b) and in mice fed a 45% HFD to evaluate its effects against lipotoxicity. First, primary hepatocytes were isolated from C57BL/6 mice and treated with various concentrations of GLE to assess toxicity. The Cell Counting Kit-8 assay showed that GLE at doses of 10, 20, or 40 mg/mL had little effect on cell viability, whereas a dose of 80 mg/mL significantly reduced viability (Fig. 6c). Therefore, non-toxic doses of GLE were used to test protection against PA-induced lipotoxicity. PA treatment reduced cell viability from 100% to 44.43 ± 6.55% compared with the vehicle control (Fig. 6d). GLE treatment increased cell viability in

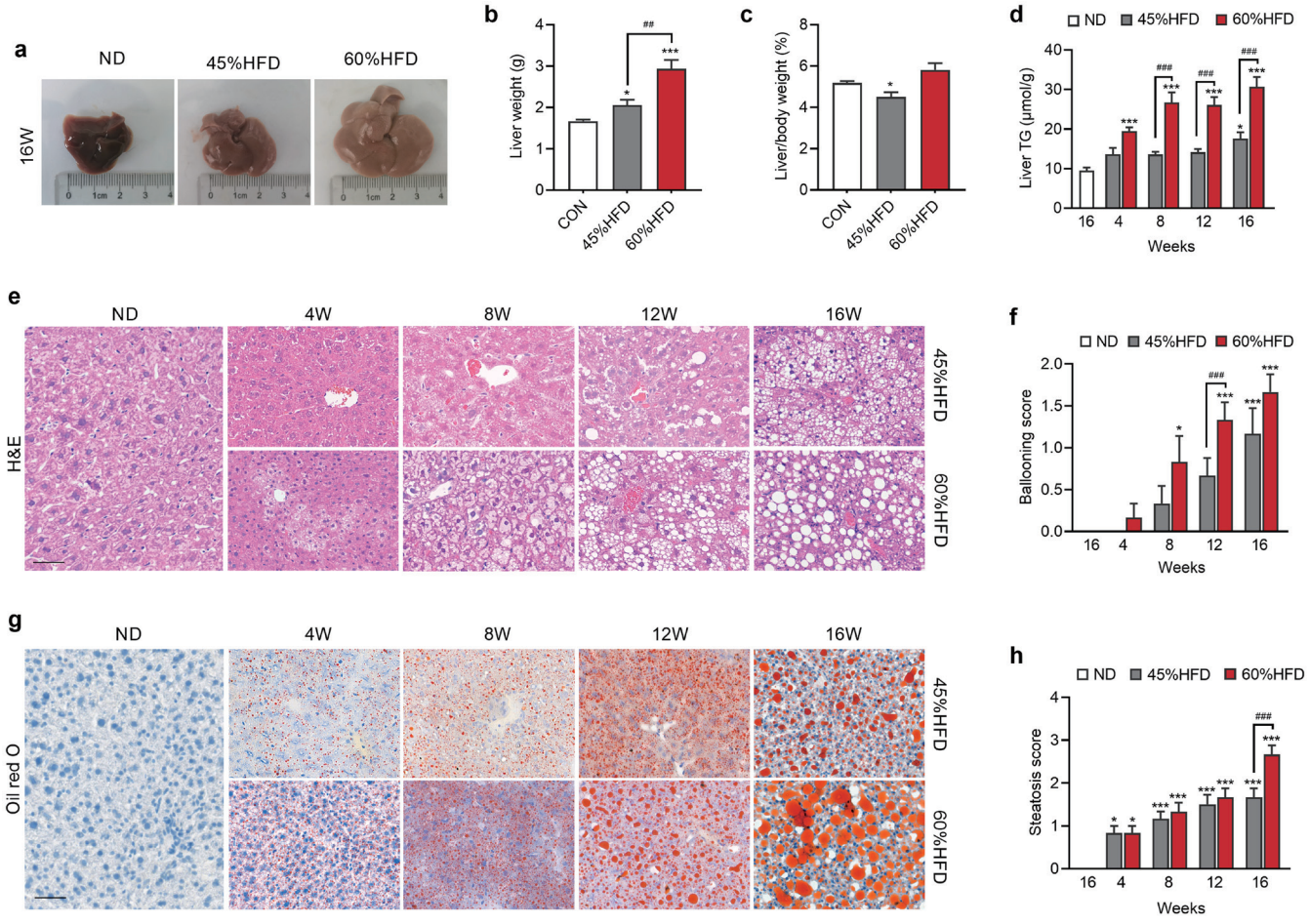

Fig. 3. Effects of different HFDs on hepatic lipid accumulation. (a) Representative macroscopic images of livers from mice fed an ND, 45% HFD, and 60% HFD. (b) Liver weight and (c) liver-to-body weight ratio at 16 weeks of ND, 45% HFD, and 60% HFD (n = 12). (d) TG content in the livers of mice. (e) Representative images of H&E-stained liver sections. (f) Ballooning scores calculated from H&E staining (n = 6). (g) Representative images of Oil Red O-stained liver sections. (h) Steatosis scores calculated from Oil Red O staining (n = 6). Scale bars, 50 μm. Data are shown as mean ± SEM. $^{*}p < 0.05$, $^{***}p < 0.001$, $^{\#\#}p < 0.01$, $^{\#\#\#}p < 0.001$. H&E, hematoxylin and eosin; HFD, high-fat diet; ND, normal chow diet; SEM, standard error of the mean; TG, triglycerides.

a dose-dependent manner, with the most significant effect observed at 40 mg/mL. Similarly, the concentrations of ALT, AST, and lactate dehydrogenase in hepatocyte culture supernatants, which indicate hepatocyte damage, significantly increased after PA treatment but were markedly reduced by GLE treatment in a dose-dependent manner (Fig. 6e–g). In addition, PA treatment induced apoptosis in primary hepatocytes, as evidenced by increased TUNEL staining (Fig. 6h and i). GLE at 40 mg/mL markedly reduced the percentage of TUNEL-positive hepatocytes, suggesting a protective effect against lipoapoptosis. GLE treatment also caused a dose-dependent reduction in phosphorylation levels of IRE1, JNK, PERK, and eIF2α compared to PA-treated hepatocytes (Fig. 6j). In mice fed a 45% HFD, GLE administration for eight weeks increased serum TG levels (Fig. 7a), decreased TC and LDL-C (Fig. 7b and c), but had no effect on HDL-C (Fig. 7d). Although GLE at 2 g/kg reduced hepatic TG levels by 24.3% compared with the 45% HFD group (Fig. 7e), hepatic TC and serum ALT levels were elevated (Fig. 7f and g), which may be attributed to the significantly increased feed intake in GLE-treated mice. Collectively, these findings demonstrate that GLE mitigates PA-induced hepatocyte damage *in vitro* and improves serum lipid profiles in HFD-fed mice.

Discussion

In general, the development of metabolic-associated diseases, such as MASLD, is a continuous and gradual process. MASLD follows a dynamic course that progresses from fatty liver to metabolic-associated steatohepatitis, with some cases advancing to cirrhosis and even hepatocellular carcinoma.[26] Here, we established and compared two mouse models that reproduce the progressive process of MASLD, accompanied by obesity and glucose and lipid metabolism disorders. Our findings demonstrate that HFD-induced lipotoxicity triggers ER stress in hepatocytes, which may activate adaptive responses including the UPR and ER-phagy. In addition, we corroborated the protective effect of GLE against lipotoxicity in primary hepatocytes and its ability to alleviate lipid metabolism disorders in a mouse model of MASLD induced by a 45% HFD.

During the initial six weeks (mouse age approximately 13 weeks), mice exhibited rapid growth, as reflected by increased body weight and lean mass, driven by elevated feed intake. After this period of rapid growth, the lean mass growth rate slowed in all mice, with no significant differences between the normal and HFD groups. Unlike lean mass, body fat in normal mice remained largely unchanged during the 16-week feeding period. In contrast, body fat in

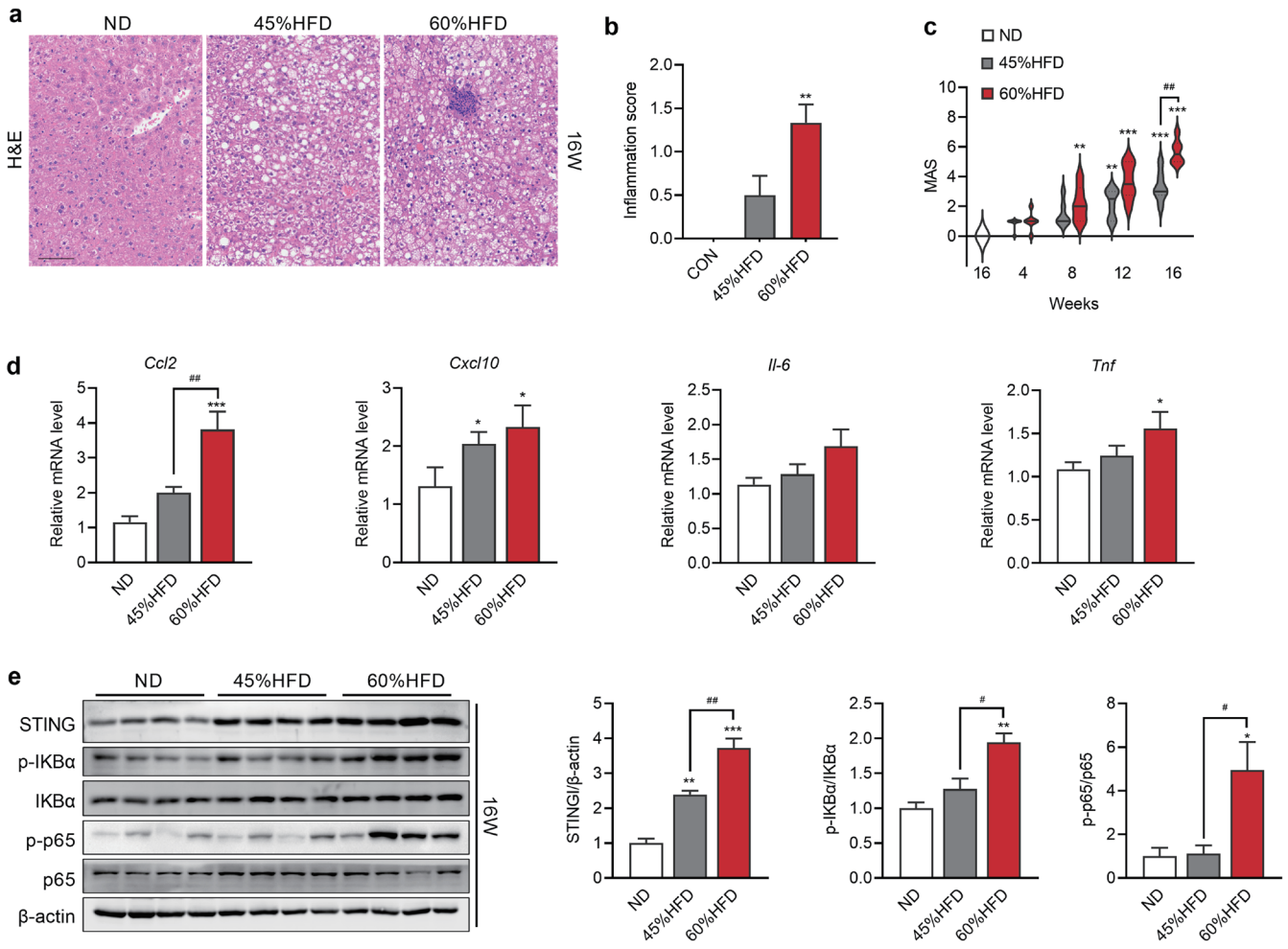

Fig. 4. Effects of different HFDs on liver inflammation. (a) Representative images of H&E-stained liver sections from mice fed ND, 45% HFD, or 60% HFD for 16 weeks. (b) Inflammation scores calculated from H&E staining. (c) MAS scores calculated from the pathological sections (n = 6). (d) Gene expression of *Ccl2*, *Cxcl10*, *Il-6*, and *Tnf* in liver tissues from mice fed the indicated diets for 16 weeks (n = 12). (e) Immunoblot analysis of STING, phosphorylated and total IKBα, p65, and corresponding densitometry (n = 4, experiments performed in triplicate). Scale bars, 50 μm. Data are shown as mean ± SEM. $^{*}p < 0.05$, $^{**}p < 0.01$, $^{***}p < 0.001$, $^{\#}p < 0.05$, $^{\#\#}p < 0.01$. *Ccl2*, C-C motif chemokine ligand 2; *Cxcl10*, C-X-C motif cchemokine ligand 10; H&E, hematoxylin and eosin; HFD, high-fat diet; *Il-6*, interleukin-6; IκBα, inhibitor of nuclear factor kappa B alpha; MAS, MASLD activity score; ND, normal chow diet; p65, transcription factor p65; SEM, standard error of the mean; STING, stimulator of interferon genes; *Tnf*, tumor necrosis factor.

HFD-fed mice continued to increase, with the weekly increment being higher in the 60% HFD group than in the 45% HFD group due to greater calorie intake. Serum lipid profiles were also altered by HFD, including increased TC, LDL-C, and HDL-C, alongside decreased TG levels. The reduction in serum TG levels after HFD feeding has also been observed in other studies.[27,28] Additionally, a meta-analysis showed that long-term HFD feeding reduced blood TG levels in overweight or obese patients.[29] Since serum TG originates from both chylomicrons secreted by the small intestine and very low-density lipoproteins secreted by the liver, the decrease in serum TG levels may reflect reduced triglyceride secretion by the small intestine in response to dietary fat challenges in obese mice.[28] Alternatively, or in combination, HFD may impair hepatic very low-density lipoprotein secretion, leading to abnormal TG accumulation in hepatocytes,[30] as also demonstrated in this study (Fig. 3d). Accumulation of TG in the liver ultimately causes lipotoxicity and inflammation as feeding is prolonged. These findings align with a recent holistic hypothesis: initially, excessive dietary fat is stored in white adipose tissue. With prolonged metabolic stress, the storage capacity of the white adipose tissues becomes overwhelmed, while lipolytic activity gradually increases, releasing excessive fatty acids into circulation. These fatty acids are then deposited in ectopic tissues such as the liver, promoting MASLD and insulin resistance.[31] The oral glucose tolerance test and the derived AUC are widely used to assess glucose tolerance.[32] Our combined glucose tolerance curve and AUC results indicate that HFD feeding profoundly impairs glucose homeostasis.

It is widely recognized that HFD-induced lipid accumulation in the liver causes ER stress in hepatocytes, contributing to the pathogenesis of metabolically driven MASLD.[33] An adaptive signaling pathway, the UPR, is activated to restore ER homeostasis.[23] In this study, two UPR branches, PERK and IRE1, were activated in the livers of mice fed HFD for 16 weeks. The extent of activation positively correlated with fat content in the different HFDs. Notably, PERK and IRE1 activation, accompanied by inflammation and hepatic damage, occurred after lipid accumulation. Beyond the canonical UPR, previous studies have demonstrated that

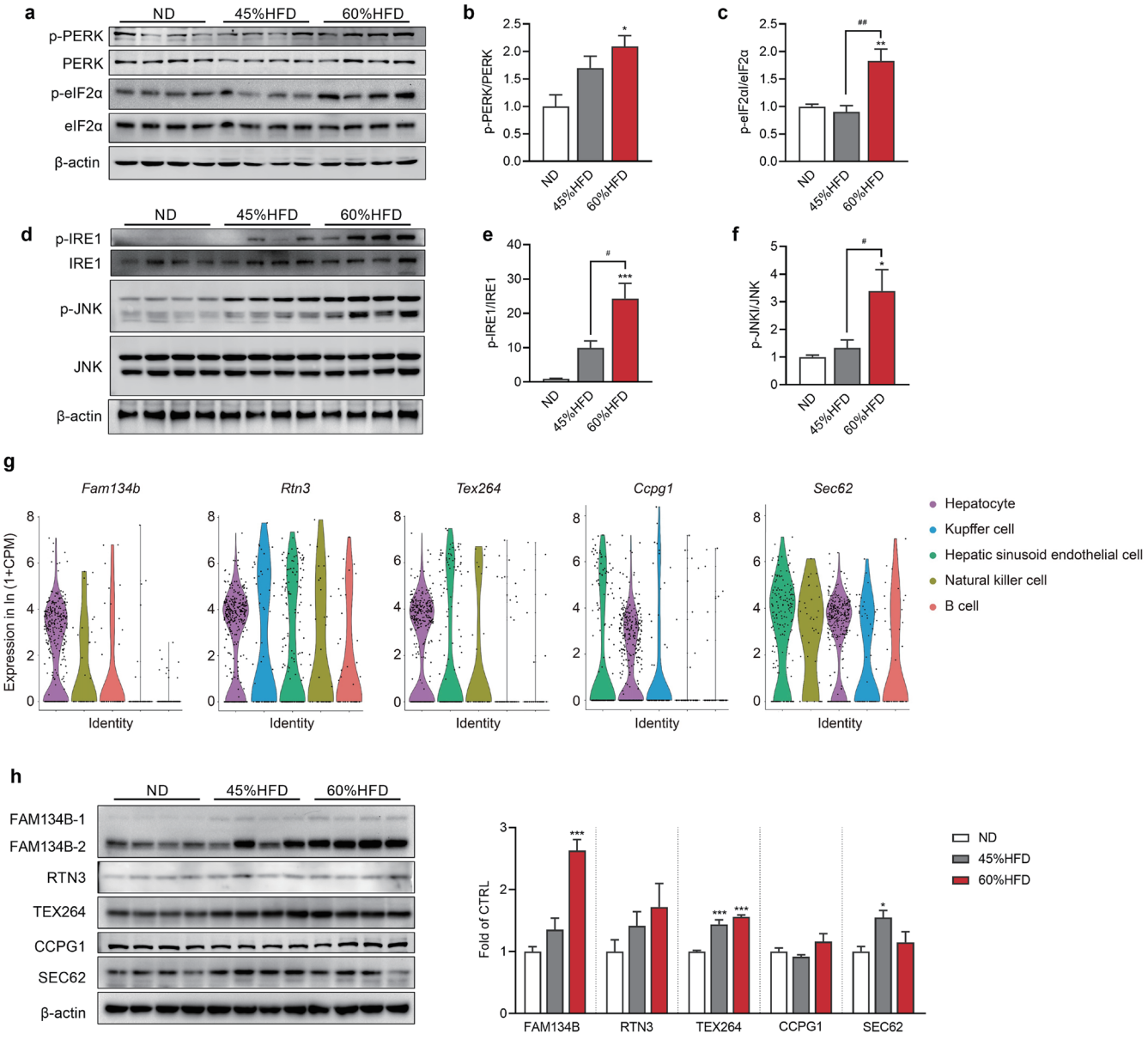

Fig. 5. Effects of different HFDs on ER stress and ER-phagy. (a) Immunoblot analysis of phosphorylated and total PERK and eIF2α, and (b, c) the corresponding densitometry (n = 4). (d) Immunoblot analysis of phosphorylated and total IRE1, JNK, and (e, f) the corresponding densitometry. (g) Single-cell transcriptome data (https://tabula-muris.ds.czbiohub.org) showing expression distribution of ER-phagy receptors in five mouse liver cell types, sorted by mean value. (h) Immunoblot analysis of FAM134B, RTN3, TEX264, CCPG1, SEC62 (left), and the corresponding densitometry (right) (n = 4). Immunoblots were performed in triplicate. Data are shown as mean ± SEM. $^{*}p < 0.05$, $^{**}p < 0.01$, $^{***}p < 0.001$, $^{\#}p < 0.05$, $^{\#\#}p < 0.01$. CCPG1, cell cycle progression 1; eIF2α, eukaryotic translation initiation factor 2 alpha; ER, endoplasmic reticulum; FAM134B, family with sequence similarity 134 member B; HFD, high-fat diet; IRE1, inositol-requiring enzyme 1; JNK, c-Jun N-terminal kinase; p-eIF2α, phosphorylated eukaryotic translation initiation factor 2 alpha; PERK, protein kinase R-like endoplasmic reticulum kinase; p-IRE1, phosphorylated IRE1; p-JNK, phosphorylated JNK; p-PERK, phosphorylated PERK; RTN3, reticulon 3; SEC62, SEC62 homolog, preprotein translocation factor; SEM, standard error of the mean; TEX264, testis-expressed protein 264.

reticulophagy, also known as ER-phagy, is induced in *in vitro* models of MASLD to alleviate ER stress, thereby restraining lipotoxicity.[8] For example, colocalization of the ER with lysosomes was observed in HepG2 cells treated with 400 μmol/L oleic acid. Our *in vivo* findings further suggest that ER-phagy receptors including FAM134B, CCPG1, SEC62, TEX264, and RTN3 are upregulated in the livers of HFD-fed mice. These results imply that ER-phagy may be activated in response to lipotoxicity, though further investigations are required to verify and elucidate the underlying mechanisms, given the multifunctional roles of these receptors. For instance, TEX264 has been reported to participate in DNA repair by acting as a co-factor of valosin-containing protein/p97 ATPase,[34] while RTN3 may induce apoptosis and contribute to inflammation resolution by interacting with tripartite motif-containing protein 25 and retinoic acid-inducible gene I during viral infection.[35–37] In addition, autophagic flux is believed to be impaired in the context of

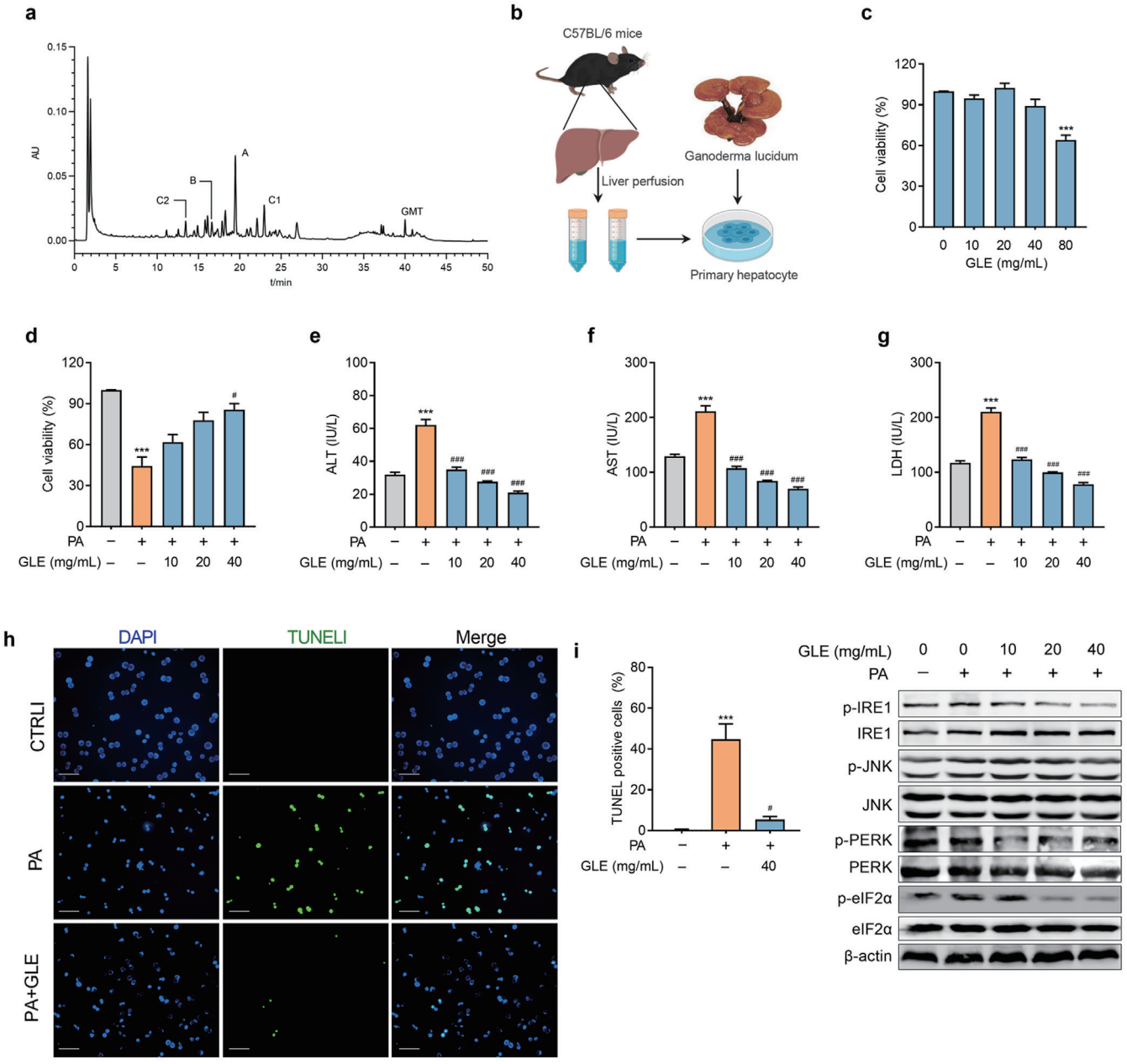

Fig. 6. GLE reduces PA-induced lipotoxicity in primary hepatocytes. (a) HPLC chromatogram of GLE. C2, B, A, and C1 represent ganoderic acids. (b) Experimental design: primary hepatocytes were isolated from eight-week-old C57BL/6 male mice. After 12 h of incubation, hepatocytes were treated with GLE in the presence or absence of PA (500 μmol/L). (c) Cell viability of primary hepatocytes treated with various concentrations of GLE (10, 20, 40, and 80 mg/mL) (n = 4). (d) Cell viability of hepatocytes treated with PA (500 μmol/L) and GLE (n = 6). ALT (d), AST (e), and LDH (f) concentrations in culture supernatants. (h) Immunofluorescence images of TUNEL (green) in hepatocytes treated with PA (500 μmol/L) and GLE (40 mg/mL); nuclei stained with Hoechst 33342 (blue). (i) Quantification of TUNEL-positive cells per field (n = 7–8 images/group). Scale bars, 50 μm. (j) Immunoblot analysis of phosphorylated and total IRE1, JNK, PERK, and eIF2α. Data are shown as mean ± SEM. $^{***}p < 0.001$, $^{\#}p < 0.05$, $^{\#\#\#}p < 0.001$. ALT, alanine aminotransferase; AST, aspartate aminotransferase; eIF2α, eukaryotic initiation factor 2 alpha; GLE, *Ganoderma lucidum* water- extract; GMT, ganodermanontriol; HPLC, high performance liquid chromatography; IRE1, inositol-requiring enzyme 1; JNK, c-Jun N-terminal kinase; LDH, lactate dehydrogenase; PA, palmitic acid; p-eIF2α, phosphorylated eIF2α; PERK, protein kinase R-like endoplasmic reticulum kinase; p-IRE1, phosphorylated inositol-requiring 1; p-JNK, phosphorylated IRE1; p-PERK, phosphorylated PERK; SEM, standard error of the mean; TUNEL, terminal deoxynucleotidyl transferase dUTP nick-end labeling.

MASLD,[38] which may explain the observed increase in ER-phagy receptors. Genetic or pharmacological interventions to manipulate autophagic flux are therefore needed to clarify this issue.

Since *G. lucidum* has demonstrated protective effects in various liver injury models, including nonalcoholic steatosis,[16] we selected this well-known Chinese herbal medicine to evaluate both *in vitro* and *in vivo* lipotoxicity models. As expected, GLE reduced PA-induced hepatocyte damage and ameliorated abnormalities in

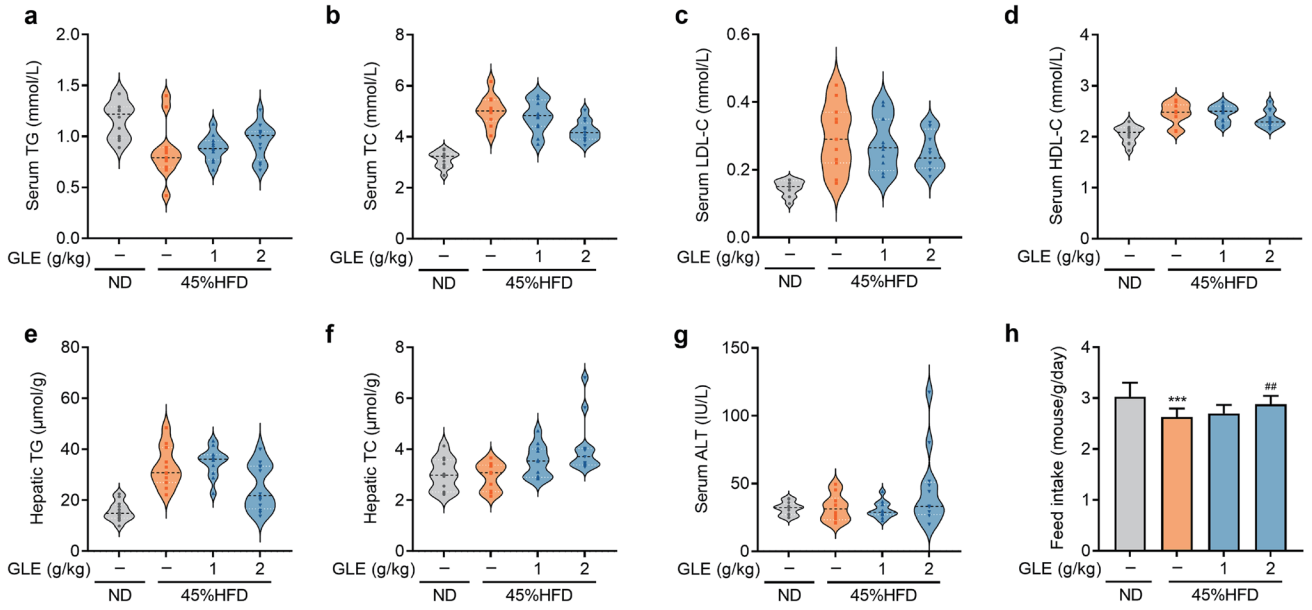

Fig. 7. Effect of GLE on mice fed a 45% HFD. Control mice were fed an ND. After four weeks of 45% HFD feeding, GLE (1 or 2 g/kg) was orally administered once daily for eight weeks. Serum TG (a), TC (b), LDL-C (c), and HDL-C (d) levels. (e, f) Hepatic TG (e) and TC (f) levels. (g) Serum ALT levels. (h) Feed intake of mice in the indicated groups. n = 12. Data are shown as mean ± SEM. $^{***}p < 0.001$, $^{\#\#}p < 0.01$. ALT, alanine aminotransferase; GLE, *Ganoderma lucidum* water- extract; HDL-C, high-density lipoprotein cholesterol; HFD, high-fat diet; LDL-C, low-density lipoprotein cholesterol; ND, normal chow diet; SEM, standard error of the mean; TC, total cholesterol; TG, total triglyceride.

serum lipid metabolism. However, mice treated with high doses of GLE displayed increased hepatic TC and serum ALT levels, suggesting potential toxicity of the extract. Although the dosage used in this study falls within the range recommended by the Chinese Pharmacopoeia and numerous studies have confirmed the low toxicity of *G. lucidum*, most toxicity research has been conducted in healthy animals.[39,40] Lipotoxicity induced by HFD may render the liver more susceptible to *G. lucidum*-induced toxic reactions, which warrants attention in future studies. Alternatively, increased feed intake induced by GLE may have diminished its protective effect against HFD-induced lipotoxicity, potentially explaining the paradoxical results. Notably, polysaccharides from *G. lucidum* have been reported to stimulate appetite under chemotherapy conditions,[41,42] consistent with our current findings.

This study has some limitations. To avoid confounding effects from cyclic estrogen fluctuations during the menstrual cycle in female animals, only male mice were used. This limits exploration of HFD impacts on ER-phagy, as well as the efficacy and potential adverse effects of GLE in females, thereby constraining clinical translation relevance.

Conclusions

Altogether, this study demonstrates that HFD-induced hepatic lipotoxicity elicits an inflammatory response along with adaptive UPR and ER-phagy, which may represent important therapeutic targets against lipotoxicity. In addition, *G. lucidum* shows protective effects against HFD-induced lipotoxicity, but its stimulatory effect on appetite should be carefully considered.

Acknowledgments

None.

Funding

This work was supported by the National Natural Science Foundation of China (82204739) and the CAMS Innovation Fund for Medical Sciences (CIFMS, 2021-I2M-1-048).

Conflict of interest

The authors declare that they have no conflicts of interest.

Author contributions

Drafting of the manuscript (CC, MY), critical review and revision (QC), data analysis (SJ, HS), methodology design (FC, YL), verification (TX, YG), and management and coordination of the research activity planning and execution (SZ). All authors have approved the final version and publication of the manuscript.

Ethical statement

All animal procedures were approved by the Animal Ethics Committee of the Institute of Medicinal Plant Development, Chinese Academy of Medical Sciences, and Peking Union Medical College (SLXD-20210930022), and conducted in accordance with the guidelines of the committee. The study protocols complied with the Animal Research: Reporting of *In Vivo* Experiments (ARRIVE) guidelines.

Data sharing statement

The data used in support of the findings of this study are available from the corresponding author upon request.

References

[1] Murru E, Manca C, Carta G, Banni S. Impact of Dietary Palmitic Acid on Lipid Metabolism. Front Nutr 2022;9:861664. doi:10.3389/fnut.2022.861664, PMID:35399673.

[2] Valenzuela PL, Carrera-Bastos P, Castillo-García A, Lieberman DE, Santos-Lozano A, Lucia A. Obesity and the risk of cardiometabolic diseases. Nat Rev Cardiol 2023;20(7):475–494. doi:10.1038/s41569-023-00847-5, PMID:36927772.

[3] Jin S, Li Y, Xia T, Liu Y, Zhang S, Hu H, *et al*. Mechanisms and therapeutic implications of selective autophagy in nonalcoholic fatty liver disease. J Adv Res 2025;67:317–329. doi:10.1016/j.jare.2024.01.027, PMID:38295876.

[4] Chew NWS, Ng CH, Tan DJH, Kong G, Lin C, Chin YH, *et al*. The global burden of metabolic disease: Data from 2000 to 2019. Cell Metab 2023;35(3):414–428.e3. doi:10.1016/j.cmet.2023.02.003, PMID:36889281.

[5] Rada P, González-Rodríguez Á, García-Monzón C, Valverde ÁM. Understanding lipotoxicity in NAFLD pathogenesis: is CD36 a key driver? Cell Death Dis 2020;11(9):802. doi:10.1038/s41419-020-03003-w, PMID:32978374.

[6] Lee AK, Kim DH, Bang E, Choi YJ, Chung HY. β-Hydroxybutyrate Suppresses Lipid Accumulation in Aged Liver through GPR109A-mediated Signaling. Aging Dis 2020;11(4):777–790. doi:10.14336/AD.2019.0926, PMID:32765945.

[7] Gubas A, Dikic I. ER remodeling via ER-phagy. Mol Cell 2022;82(8):1492–1500. doi:10.1016/j.molcel.2022.02.018, PMID:35452617.

[8] Pang L, Liu K, Liu D, Lv F, Zang Y, Xie F, *et al*. Differential effects of reticulophagy and mitophagy on nonalcoholic fatty liver disease. Cell Death Dis 2018;9(2):90. doi:10.1038/s41419-017-0136-y, PMID:29367738.

[9] Ahmad MF. Ganoderma lucidum: Persuasive biologically active constituents and their health endorsement. Biomed Pharmacother 2018;107:507–519. doi:10.1016/j.biopha.2018.08.036, PMID:30114634.

[10] Wang J, Cao B, Zhao H, Feng J. Emerging Roles of Ganoderma Lucidum in Anti-Aging. Aging Dis 2017;8(6):691–707. doi:10.14336/AD.2017.0410, PMID:29344411.

[11] Yu Q, Nie SP, Wang JQ, Huang DF, Li WJ, Xie MY. Signaling pathway involved in the immunomodulatory effect of Ganoderma atrum polysaccharide in spleen lymphocytes. J Agric Food Chem 2015;63(10):2734–2740. doi:10.1021/acs.jafc.5b00028, PMID:25715057.

[12] Li WJ, Tang XF, Shuai XX, Jiang CJ, Liu X, Wang LF, *et al*. Mannose Receptor Mediates the Immune Response to Ganoderma atrum Polysaccharides in Macrophages. J Agric Food Chem 2017;65(2):348–357. doi:10.1021/acs.jafc.6b04888, PMID:27931102.

[13] Wang K, Bao L, Ma K, Zhang J, Chen B, Han J, *et al*. A novel class of α-glucosidase and HMG-CoA reductase inhibitors from Ganoderma leucocontextum and the anti-diabetic properties of ganomycin I in KK-A(y) mice. Eur J Med Chem 2017;127:1035–1046. doi:10.1016/j.ejmech.2016.11.015, PMID:27839787.

[14] Yang Z, Wu F, He Y, Zhang Q, Zhang Y, Zhou G, *et al*. A novel PTP1B inhibitor extracted from Ganoderma lucidum ameliorates insulin resistance by regulating IRS1-GLUT4 cascades in the insulin signaling pathway. Food Funct 2018;9(1):397–406. doi:10.1039/c7fo01489a, PMID:29215104.

[15] Li L, Guo WL, Zhang W, Xu JX, Qian M, Bai WD, *et al*. Grifola frondosa polysaccharides ameliorate lipid metabolic disorders and gut microbiota dysbiosis in high-fat diet fed rats. Food Funct 2019;10(5):2560–2572. doi:10.1039/c9fo00075e, PMID:30994668.

[16] Jung S, Son H, Hwang CE, Cho KM, Park SW, Kim HJ. Ganoderma lucidum Ameliorates Non-Alcoholic Steatosis by Upregulating Energy Metabolizing Enzymes in the Liver. J Clin Med 2018;7(6):152. doi:10.3390/jcm7060152, PMID:29914094.

[17] Guo WL, Guo JB, Liu BY, Lu JQ, Chen M, Liu B, *et al*. Ganoderic acid A from Ganoderma lucidum ameliorates lipid metabolism and alters gut microbiota composition in hyperlipidemic mice fed a high-fat diet. Food Funct 2020;11(8):6818–6833. doi:10.1039/d0fo00436g, PMID:32686808.

[18] Klupp NL, Kiat H, Bensoussan A, Steiner GZ, Chang DH. A double-blind, randomised, placebo-controlled trial of Ganoderma lucidum for the treatment of cardiovascular risk factors of metabolic syndrome. Sci Rep 2016;6:29540. doi:10.1038/srep29540, PMID:27511742.

[19] Kennard MR, Nandi M, Chapple S, King AJ. The glucose tolerance test in mice: Sex, drugs and protocol. Diabetes Obes Metab 2022;24(11):2241–2252. doi:10.1111/dom.14811, PMID:35815375.

[20] Yan M, Jin S, Wang Z, Xia T, Liu Y, Chang Q. Limonin counteracts obesity by activating thermogenesis in brown and white adipose tissues. J Funct Foods 2023;100:105393. doi:10.1016/j.jff.2022.105393.

[21] Kleiner DE, Brunt EM, Van Natta M, Behling C, Contos MJ, Cummings OW, *et al*. Design and validation of a histological scoring system for nonalcoholic fatty liver disease. Hepatology 2005;41(6):1313–1321. doi:10.1002/hep.20701, PMID:15915461.

[22] Yan M, Jin S, Liu Y, Wang L, Wang Z, Xia T, *et al*. Cajaninstilbene Acid Ameliorates Acetaminophen-Induced Liver Injury Through Enhancing Sestrin2/AMPK-Mediated Mitochondrial Quality Control. Front Pharmacol 2022;13:824138. doi:10.3389/fphar.2022.824138, PMID:35350766.

[23] Lebeaupin C, Vallée D, Hazari Y, Hetz C, Chevet E, Bailly-Maitre B. Endoplasmic reticulum stress signalling and the pathogenesis of non-alcoholic fatty liver disease. J Hepatol 2018;69(4):927–947. doi:10.1016/j.jhep.2018.06.008, PMID:29940269.

[24] Wen Z, Sun Q, Shan Y, Xie W, Ding Y, Wang W, *et al*. Endoplasmic Reticulum Stress in Osteoarthritis: A Novel Perspective on the Pathogenesis and Treatment. Aging Dis 2023;14(2):283–286. doi:10.14336/AD.2022.0725, PMID:37008062.

[25] Da J, Wu WY, Hou JJ, Long HL, Yao S, Yang Z, *et al*. Comparison of two officinal Chinese pharmacopoeia species of Ganoderma based on chemical research with multiple technologies and chemometrics analysis. J Chromatogr A 2012;1222:59–70. doi:10.1016/j.chroma.2011.12.017, PMID:22226558.

[26] Friedman SL, Neuschwander-Tetri BA, Rinella M, Sanyal AJ. Mechanisms of NAFLD development and therapeutic strategies. Nat Med 2018;24(7):908–922. doi:10.1038/s41591-018-0104-9, PMID:29967350.

[27] Tsai JY, Kienesberger PC, Pulinilkunnil T, Sailors MH, Durgan DJ, Villegas-Montoya C, *et al*. Direct regulation of myocardial triglyceride metabolism by the cardiomyocyte circadian clock. J Biol Chem 2010;285(5):2918–2929. doi:10.1074/jbc.M109.077800, PMID:19940111.

[28] Uchida A, Whitsitt MC, Eustaquio T, Slipchenko MN, Leary JF, Cheng JX, *et al*. Reduced triglyceride secretion in response to an acute dietary fat challenge in obese compared to lean mice. Front Physiol 2012;3:26. doi:10.3389/fphys.2012.00026, PMID:22375122.

[29] Schwingshackl L, Hoffmann G. Comparison of effects of long-term low-fat vs high-fat diets on blood lipid levels in overweight or obese patients: a systematic review and meta-analysis. J Acad Nutr Diet 2013;113(12):1640–1661. doi:10.1016/j.jand.2013.07.010, PMID:24139973.

[30] Fang W, Chen Q, Cui K, Chen Q, Li X, Xu N, *et al*. Lipid overload impairs hepatic VLDL secretion via oxidative stress-mediated PKCδ-HNF4α-MTP pathway in large yellow croaker (Larimichthys crocea). Free Radic Biol Med 2021;172:213–225. doi:10.1016/j.freeradbiomed.2021.06.001, PMID:34116177.

[31] Loomba R, Friedman SL, Shulman GI. Mechanisms and disease consequences of nonalcoholic fatty liver disease. Cell 2021;184(10):2537–2564. doi:10.1016/j.cell.2021.04.015, PMID:33989548.

[32] Cobelli C, Dalla Man C, Toffolo G, Basu R, Vella A, Rizza R. The oral minimal model method. Diabetes 2014;63(4):1203–1213. doi:10.2337/db13-1198, PMID:24651807.

[33] Pagliassotti MJ. Endoplasmic reticulum stress in nonalcoholic fatty liver disease. Annu Rev Nutr 2012;32:17–33. doi:10.1146/annurev-nutr-071811-150644, PMID:22809102.

[34] Fielden J, Wiseman K, Torrecilla I, Li S, Hume S, Chiang SC, *et al*. TEX264 coordinates p97- and SPRTN-mediated resolution of topoisomerase 1-DNA adducts. Nat Commun 2020;11(1):1274. doi:10.1038/s41467-020-15000-w, PMID:32152270.

[35] Xiang R, Zhao S. RTN3 inducing apoptosis is modulated by an adhesion protein CRELD1. Mol Cell Biochem 2009;331(1-2):225–230. doi:10.1007/s11010-009-0163-9, PMID:19521671.

[36] Lee JT, Lee TJ, Kim CH, Kim NS, Kwon TK. Over-expression of Reticulon 3 (RTN3) enhances TRAIL-mediated apoptosis via up-regulation

of death receptor 5 (DR5) and down-regulation of c-FLIP. Cancer Lett 2009;279(2):185–192. doi:10.1016/j.canlet.2009.01.035, PMID:19250737.

[37] Yang Z, Wang J, He B, Zhang X, Li X, Kuang E. RTN3 inhibits RIG-I-mediated antiviral responses by impairing TRIM25-mediated K63-linked polyubiquitination. Elife 2021;10:e68958. doi:10.7554/eLife.68958, PMID:34313226.

[38] Tanaka S, Hikita H, Tatsumi T, Sakamori R, Nozaki Y, Sakane S, *et al*. Rubicon inhibits autophagy and accelerates hepatocyte apoptosis and lipid accumulation in nonalcoholic fatty liver disease in mice. Hepatology 2016;64(6):1994–2014. doi:10.1002/hep.28820, PMID:27637015.

[39] Meneses ME, Martínez-Carrera D, González-Ibáñez L, Torres N, Sánchez-Tapia M, Márquez-Mota CC, *et al*. Effects of Mexican Ganoderma lucidum extracts on liver, kidney, and the gut microbiota of Wistar rats: A repeated dose oral toxicity study. PLoS One 2023;18(4):e0283605. doi:10.1371/journal.pone.0283605, PMID:37022999.

[40] Zhang J, Gao X, Pan Y, Xu N, Jia L. Toxicology and immunology of Ganoderma lucidum polysaccharides in Kunming mice and Wistar rats. Int J Biol Macromol 2016;85:302–310. doi:10.1016/j.ijbiomac.2015.12.090, PMID:26763176.

[41] Wu SY, Ou CC, Lee ML, Hsin IL, Kang YT, Jan MS, *et al*. Polysaccharide of Ganoderma lucidum Ameliorates Cachectic Myopathy Induced by the Combination Cisplatin plus Docetaxel in Mice. Microbiol Spectr 2023;11(3):e0313022. doi:10.1128/spectrum.03130-22, PMID:37212664.

[42] Jeitler M, Michalsen A, Frings D, Hübner M, Fischer M, Koppold-Liebscher DA, *et al*. Significance of Medicinal Mushrooms in Integrative Oncology: A Narrative Review. Front Pharmacol 2020;11:580656. doi:10.3389/fphar.2020.580656, PMID:33424591.